

RESEARCH

Open Access



Beyond just “flattening the curve”: Optimal control of epidemics with purely non-pharmaceutical interventions

Markus Kantner^{1*}  and Thomas Koprucki¹ 

*Correspondence:

kantner@wias-berlin.de

¹Weierstrass Institute for Applied
Analysis and Stochastics (WIAS),
Mohrenstr. 39, Berlin, 10117,
Germany

Abstract

When effective medical treatment and vaccination are not available, non-pharmaceutical interventions such as social distancing, home quarantine and far-reaching shutdown of public life are the only available strategies to prevent the spread of epidemics. Based on an extended SEIR (susceptible-exposed-infectious-recovered) model and continuous-time optimal control theory, we compute the optimal non-pharmaceutical intervention strategy for the case that a vaccine is never found and complete containment (eradication of the epidemic) is impossible. In this case, the optimal control must meet competing requirements: First, the minimization of disease-related deaths, and, second, the establishment of a sufficient degree of natural immunity at the end of the measures, in order to exclude a second wave. Moreover, the socio-economic costs of the intervention shall be kept at a minimum. The numerically computed optimal control strategy is a single-intervention scenario that goes beyond heuristically motivated interventions and simple “flattening of the curve”. Careful analysis of the computed control strategy reveals, however, that the obtained solution is in fact a tightrope walk close to the stability boundary of the system, where socio-economic costs and the risk of a new outbreak must be constantly balanced against one another. The model system is calibrated to reproduce the initial exponential growth phase of the COVID-19 pandemic in Germany.

MSC: 92D30; 37N25; 37N40; 93C10; 49N90; 34B15

Keywords: Mathematical epidemiology; Optimal control; Non-pharmaceutical interventions; Reproduction number; Dynamical systems; COVID-19; SARS-CoV2

1 Introduction

Preventing the spread of new diseases, to which there is no immunity in the population, is a huge problem, since there are often neither vaccines nor other effective medical treatments available in the early stages. In this case, non-pharmaceutical interventions (NPIs) such as intensive hand hygiene, home quarantine and measures of social distancing, e.g. closure of schools, universities and shops, prohibition of mass events up to curfew and shutdown of entire territories, are the only available measures. The NPIs are aimed at

© The Author(s) 2020. This article is licensed under a Creative Commons Attribution 4.0 International License, which permits use, sharing, adaptation, distribution and reproduction in any medium or format, as long as you give appropriate credit to the original author(s) and the source, provide a link to the Creative Commons licence, and indicate if changes were made. The images or other third party material in this article are included in the article's Creative Commons licence, unless indicated otherwise in a credit line to the material. If material is not included in the article's Creative Commons licence and your intended use is not permitted by statutory regulation or exceeds the permitted use, you will need to obtain permission directly from the copyright holder. To view a copy of this licence, visit <http://creativecommons.org/licenses/by/4.0/>.

“flattening the curve”, i.e., a reduction of the transmission rate in order to break the exponential growth of the epidemic.

In the case of the currently spreading COVID-19 pandemic caused by the new SARS-CoV2 coronavirus [1, 2], the fundamental concern of the mitigation measures is not to exceed the available number of intensive care unit (ICU) beds, in particular for respiratory support or extracorporeal membrane oxygenation, in order to prevent actually avoidable deaths [3]. Since the outbreak of the epidemic, a large number of simulation studies have been conducted using mathematical models to assess the efficacy of different NPIs and to estimate the corresponding demands on the health care system [4–12]. Moreover, mathematical models are employed to deduce important epidemiological parameters [13–15] and to evaluate the effect of particular measures from empirical data [16, 17].

The vast majority of research papers on the control of COVID-19 examines the impact of rather simple intervention schemes such as bang-bang control or cascaded on-off (i.e., repeated lockdown and release) strategies [12, 18–20]. Instead, however, intervention strategies derived from continuous-time optimal control theory [21] following a variational principle are actually preferable. There is a large number of studies on the application of optimal control theory following Pontryagin’s maximum principle [22] in mathematical epidemiology, see Refs. [23–27] and references therein. The by far largest part of these works deals with optimal control of epidemics through vaccination and immunization [28–31], medical treatment [32, 33] and combinations thereof [34–39]. Significantly fewer papers are concerned with the optimal control of transmission dynamics and the mitigation of epidemics through social distancing measures. The paper by Behncke [25] studies the optimal control of transmission dynamics via optimally steered health-promotion campaigns and seems to be one of the first works devoted to this problem. During the current COVID-19 pandemic, the control of the disease by NPIs has moved into the focus of attention and a number of recent papers are devoted to this problem. Djidjou-Demasse et al. [40] investigated the optimal control of the epidemic via social distancing and lockdown measures until a vaccine becomes available. They propose to delay the peak of the epidemic by increasingly strict interventions and finally to relax the measures in such a way that a significant burden on the health care system only occurs when the availability of a vaccine is already expected. A similar problem has been considered by Perkins and España [41], who studied the optimal implementation of NPIs under the assumption that an effective vaccine would become available in about one year after the outbreak of the epidemic. The paper by Kruse and Strack [42] is devoted to the analysis of the optimal timing of social distancing measures under the constraint that the overall (temporal) budget for NPIs is limited. Ketcheson [43] presented a detailed analysis for optimal transmission control in a SIR (susceptible-infected-recovered) epidemic model with the aim of achieving a stable equilibrium (“herd immunity”) within a fixed finite time interval while simultaneously avoiding hospital overflow. A similar problem (including a simple state-dependent mortality rate) was studied by Alvarez et al. [44], who focussed on minimizing the lockdown costs and included further economic aspects such as the assumed value of statistical life. An extension of the optimal transmission control problem to an age-structured model has been presented by Bonnans and Gianatti [45], who proposed a different temporal course of the contact reduction for the high and low risk sub-populations. Köhler et al. [46] have applied model predictive control to social distancing measures with the objective of minimizing the fatalities over a fixed period of time of two

years. Next to adaptive feedback strategies for iterative loosening of the social distancing policies after an initial lockdown, the authors also examined the possibility of eradicating the virus. All of these papers on optimal control deal with deterministic epidemiological models, in particular the basic SIR model [25, 42–44, 47] or various extended SEIR-type models [40, 41, 46]. We remark that this survey on optimal control of COVID-19 is not exhaustive.

The objective of this paper is the investigation of the optimal control of epidemics in the (hopefully unlikely) case in which an effective vaccine is impossible or never found and the epidemic must be controlled with purely non-pharmaceutical measures. Furthermore, we exclude the possibility of complete containment (“eradication of the virus”). Then, optimal control must pursue competing objectives: On the one hand, the number of disease-related deaths shall be minimized by strictly avoiding an overload of the intensive care treatment capacities. On the other hand, however, sufficient natural immunity must be established in the population in the long run to prevent a second outbreak of the epidemic (“herd immunity”). Moreover, the socio-economic costs of the intervention shall be kept at a minimum. We compute the optimal solution to this problem by applying Pontryagin’s Maximum Principle to an extended SEIR-type model tailored to specific aspects of COVID-19. Our main result is the optimal time course of the mean contact reduction (and the corresponding time-dependent effective reproduction number) that serves as a guideline on how to optimally enter and finally exit the lockdown. The corresponding NPI policy is a single-intervention scenario that can be divided into three distinct phases: (1) a strict initial lockdown, (2) a long lasting period (“critical period”) during which the number of active cases is kept approximately constant and (3) a moderate tightening of the measures towards the end of the intervention. We present a detailed analysis of the numerically computed result and develop an analytical understanding of its distinct features. Moreover, we show that our numerically computed optimal control obeys two fundamental stability criteria, which impose an upper limit on the transmission rate and its rate of change on the way out of the initial lockdown. The precise structure of the optimal control (i.e., three phases of the intervention) obtained in this paper differs from the results described in similar works [42–44]. After the initial submission of this paper, the preprint by Charpentier et al. [48] appeared, who studied a similar optimization problem on the basis of an extended SIR-type model with parameters adjusted to the COVID-19 pandemic in France. Their independently obtained results are comparable to those presented in this paper, which demonstrates the robustness of the obtained optimal intervention strategy with respect to model and parameter variations.

The mathematical model for the progression of the epidemic and the estimation of the demand for intensive care resources is described in Sect. 2. The optimal control problem is derived in Sect. 3 and the results are described in Sect. 4. We close with a critical discussion of our findings in Sect. 5. The model has been calibrated to reproduce the exponential growth phase of the COVID-19 pandemic in Germany. Details on the parameter adjustment are described in the [Appendix](#).

2 Modeling of disease spreading and demand for intensive care units

Mathematical modeling of the spread of epidemics is an indispensable tool to project the outcome of an epidemic, estimate important epidemiological parameters and to make predictions for different intervention scenarios. Compartment models [49–51], where

the population is divided into different macroscopic sub-populations, such as *susceptible, infectious, recovered* etc., are a simple but effective tool to model the progression of epidemics. In contrast to complex (but more realistic) stochastic agent-based models [52, 53], deterministic mean-field models are limited to the description of the average infection dynamics in macroscopic (sub-)populations, but allow for fast parameter scans and a straightforward application of continuous-time optimal control theory [21].

2.1 Model equations

In this paper, an extended SEIR model, similar to that proposed by Neher et al. [54, 55], is used to model the spread of an epidemic and to estimate the number of patients in a critical state that require intensive care. Similar models are described in Refs. [14, 46, 56]. For the sake of simplicity, vital dynamics (except for disease-related deaths), seasonality effects [57], dispersion of transmission [58] and any effects caused by population heterogeneity (different age and risk groups) are neglected. The total population is divided into distinct compartments: susceptible S , exposed E , infectious I , hospitalized H (severely ill), critical C , recovered R (i.e., immune) and deceased D . The model equations read

$$\dot{S} = -\beta u(t) \frac{IS}{N}, \quad (1a)$$

$$\dot{E} = \beta u(t) \frac{IS}{N} - \gamma_l E, \quad (1b)$$

$$\dot{I} = \gamma_l E - \gamma_i I, \quad (1c)$$

$$\dot{H} = (1 - m)\gamma_i I + (1 - f(C/C_0))\gamma_c C - \gamma_h H, \quad (1d)$$

$$\dot{C} = c\gamma_h H - \gamma_c C, \quad (1e)$$

$$\dot{R} = m\gamma_i I + (1 - c)\gamma_h H, \quad (1f)$$

$$\dot{D} = f(C/C_0)\gamma_c C. \quad (1g)$$

The group of initially healthy and not yet infected (susceptible, S) is vulnerable to infection through contact with infectious (I), who may transmit the disease to the susceptible population. The infection probability is determined by the transmission rate β , and the share of the susceptible and infectious population on the total (living) population $N = N(t)$, which is given as

$$N = S + E + I + H + C + R. \quad (2)$$

The newly infected (exposed, E) become infectious themselves only after a latency period γ_l^{-1} (which must not be confused with the incubation time). The infectious either recover or turn severely ill after an average period γ_i^{-1} . Severely ill (H) can either deteriorate into a critical state (C) or recover after a period γ_h^{-1} . The recovered population (R) is assumed to be immune against new infections. Patients in a critical state either stabilize to the severely ill state or die from the disease on a time scale γ_c^{-1} . The disease-related deaths reduce the size of the population

$$\dot{N} = -\dot{D}, \quad (3)$$

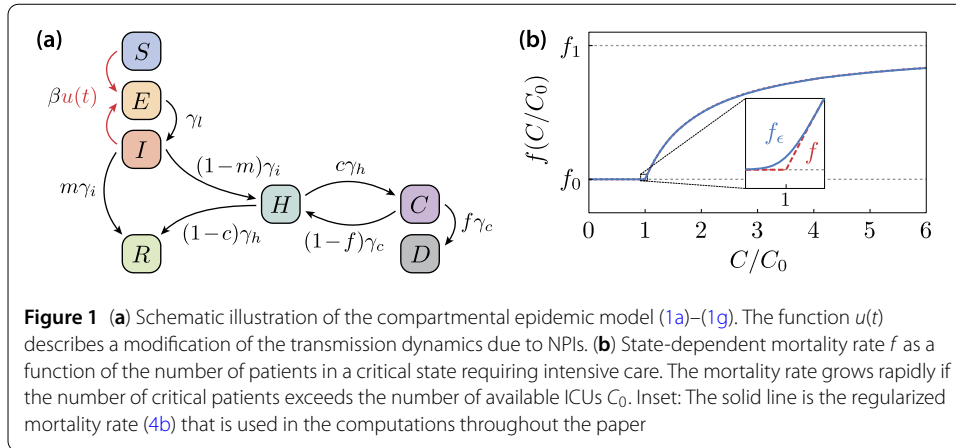


Figure 1 (a) Schematic illustration of the compartmental epidemic model (1a)–(1g). The function $u(t)$ describes a modification of the transmission dynamics due to NPIs. (b) State-dependent mortality rate f as a function of the number of patients in a critical state requiring intensive care. The mortality rate grows rapidly if the number of critical patients exceeds the number of available ICUs C_0 . Inset: The solid line is the regularized mortality rate (4b) that is used in the computations throughout the paper

such that, assuming initially $D(0) = 0$, it holds $N(t) = N(0) - D(t)$. Moreover, m is the share of infectious that are asymptomatic or have at most mild symptoms, c is the fraction of severely ill that become critical and f is the fraction of critically ill that are going to die from the disease. Finally, the time-dependent function $u(t)$ describes a modification of the transmission rate (mean contact reduction) due to NPIs. Here, $u = 1$ means no intervention, and $u = 0$ corresponds to the extreme case of total isolation of the whole population. The model system is illustrated in Fig. 1(a). A rescaled version of the dynamical system (1a)–(1g), where the sub-populations are considered in terms of their relative share of the initial population $N(0)$, is given in Eq. (23a)–(23g) in the Appendix D.

2.2 State-dependent fatality rate

The disease-related mortality grows tremendously as soon as the number of critically ill exceeds the capacity limit C_0 of the health care system (number of available ICUs). This is modeled by a state-dependent average fatality rate

$$f = f\left(\frac{C}{C_0}\right) = \begin{cases} f_0 & \text{for } C \leq C_0, \\ f_1 - \frac{C_0}{C}(f_1 - f_0) & \text{for } C > C_0. \end{cases} \tag{4a}$$

As long as every critical patient can be served with an ICU ($C \leq C_0$), the fatality rate is a constant $f = f_0$. As soon as the ICU resources are exceeded, an increasing fraction of the critical patients dies with a higher rate $f_1 > f_0$, which on average results in the state-dependent fatality rate (4a). Here, $f_1 = 2f_0$ is assumed. In the following, the regularization

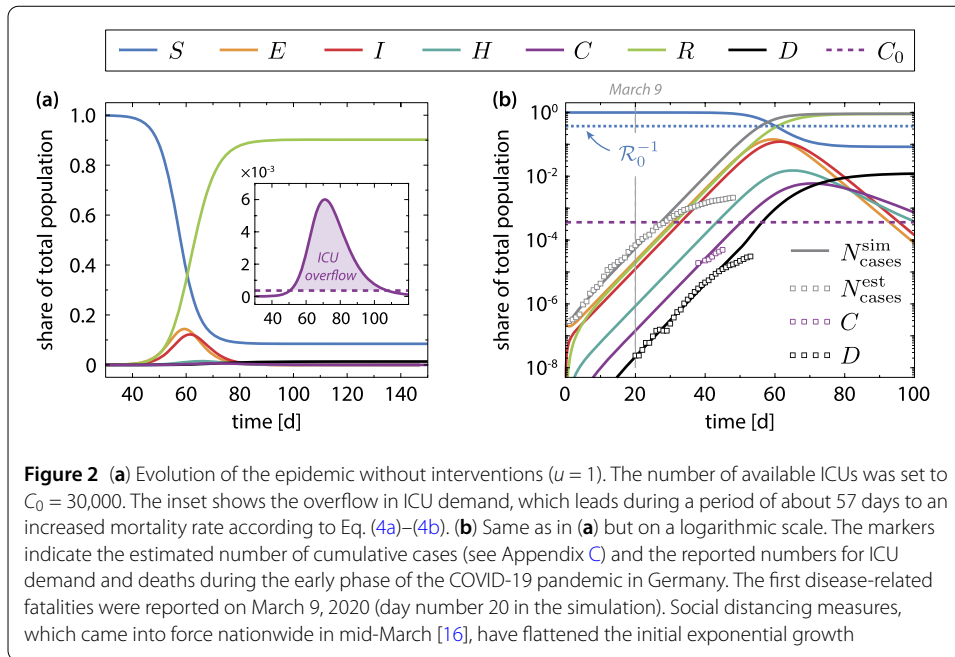
$$f(x) \rightarrow f_\epsilon(x) = f_0 + \frac{\epsilon}{x + 1.1\epsilon} \log\left(1 + \exp\left(\frac{x-1}{\epsilon}\right)\right)(f_1 - f_0) \tag{4b}$$

with $0 < \epsilon \ll 1$, of Eq. (4a) is used, in order to avoid problems due to the non-differentiability at $C = C_0$. The function $f(C/C_0)$ is plotted in Fig. 1(b).

2.3 Basic and effective reproduction number

The basic reproduction number [59]

$$\mathcal{R}_0 = \beta/\gamma_i \tag{5}$$



can be thought of as the expected number of cases (without intervention, $u = 1$) that is directly generated by one case in a population where all individuals are susceptible to infection. The effective reproduction number

$$\mathcal{R}_{\text{eff}}(t) = \mathcal{R}_0 u(t) S(t) / N(t) \tag{6}$$

depends on time and includes the impact of intervention measures.

2.4 Numerical results for the uncontrolled epidemic (COVID-19 in Germany)

Figure 2 shows the progression of an uncontrolled epidemic starting from an initially small fraction of exposed population. The initial conditions are listed in Appendix D. The parameters are adjusted (see Appendix C) to reproduce the initial exponential growth phase of the COVID-19 disease in Germany (late February – mid March 2020) and are summarized in Table 1. The numerical solution was obtained by a 4th order Runge–Kutta method. Without intervention, the peak number of simultaneously active cases is about 23 million and the peak number of patients in a critical state exceeds the number of ICUs by a factor of about $C_{\text{max}}/C_0 \approx 16.7$, see inset of Fig. 2(a). The simulated value $C_{\text{max}} \approx 5.0 \times 10^5$ is in very good agreement with the projection by Khailaie et al. [14]. Due to the increased fatality in the period with ICU overflow, see Eq. (4a)–(4b), the epidemic terminates with a very high number of deaths $D(T) \approx 1.0 \times 10^6$, which is in line with previous studies [11].

3 Optimal control

In the scenario outlined in Sect. 1, where an effective vaccine is never found, the optimal transmission control due to NPIs is required (i) to avoid ICU overflow (more patients in a critical state than available ICUs) but at the same time (ii) exclude a second wave of the epidemic after the end of the measures. The optimal solution is computed by minimizing

Table 1 List of parameters used in the simulations. See Appendix C for details

Symbol	Value	Description
\mathcal{R}_0	2.7	basic reproduction number
$N(0)$	83×10^6	initial population size
γ_l^{-1}	2.6d	average latency time between exposure and infectious period
γ_i^{-1}	2.35d	average infectious period before recovery or hospitalization
γ_h^{-1}	4.0d	average period before severely ill patients turn critical or recover
γ_c^{-1}	7.5d	average period before critical patients recover or die
β	$(1.15\text{d})^{-1}$	transmission rate
m	0.92	fraction of infected with at most mild symptoms
c	0.27	fraction of hospitalized patients that turn critical
f	see Eq. (4a)–(4b)	fraction of critical patients that turn fatal
f_0	0.31	mortality of a critical patient with ICU
f_1	$2 f_0 = 0.62$	mortality of a critical patient without ICU
C_0	variable	number of ICUs/ max. number of simultaneously critical cases
T	$10 \times T_{\text{crit}}$	final time of the simulation, for T_{crit} see Eq. (17)

the index functional

$$\mathcal{J}[u] = \varphi(\mathbf{x}(T)) + \int_0^T dt \mathcal{C}(u(t)), \quad (7a)$$

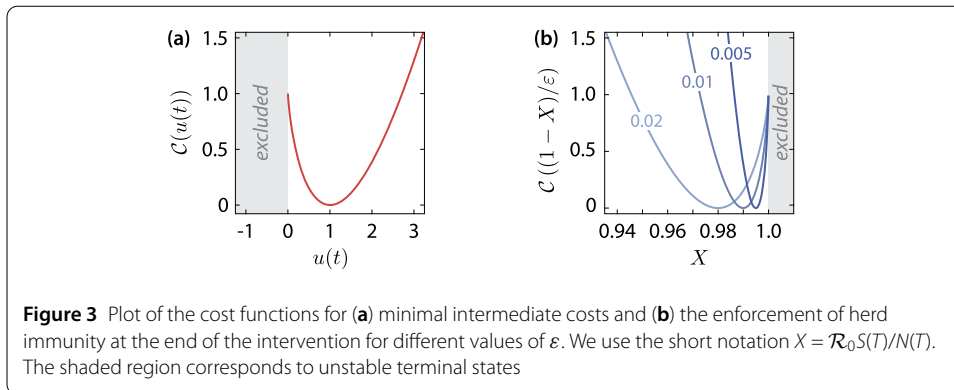
where

$$\varphi(\mathbf{x}(T)) = \mathcal{P}D(T) + \mathcal{C}\left(\frac{1}{\varepsilon}\left(1 - \mathcal{R}_0 \frac{S(T)}{N(T)}\right)\right) \quad (7b)$$

is the terminal cost function. The first term in Eq. (7b) describes the number of disease-related deaths $D(T)$ at the end of the epidemic, which should be minimized. As the increment of the disease-related deaths depends on the state-dependent fatality rate, see Eq. (1g), this condition implies that the ICU capacities must not be exceeded. The second term in Eq. (7b) controls the size of the susceptible population $S(T)$ at the end of the epidemic. In order to approach a stable, disease-free stationary state (“herd immunity”), the share of susceptibles on the total population must be less than \mathcal{R}_0^{-1} at the end of the intervention, see Appendix A. The term in Eq. (7b) enforces a final state slightly below the stability boundary (just in the stable regime), where $0 < \varepsilon \ll 1$ is a small parameter. We use $\varepsilon = 10^{-2}$ in the numerical simulations throughout this paper. The function

$$\mathcal{C}(x) = x \log(x) - x + 1 \quad (8)$$

is convex on the whole domain $x \in [0, \infty)$. It appears also in the last term of Eq. (7a) as an intermediate cost function, which provides an abstract measure for the total socio-economic costs caused by the intervention. The term is minimal and zero if no intervention is applied $\mathcal{C}(1) = \mathcal{C}'(1) = 0$, see Fig. 3. The advantage of using (8) over the commonly used quadratic cost functions is that “unphysical” negative values of u are a priori excluded. The control parameter \mathcal{P} balances between the competing objectives of minimal disease-related deaths (first term), while attaining at the same time a minimum number of cases to enforce $S(T)$ slightly below the stability boundary (second term). Ramping up \mathcal{P} puts an increasing emphasis on minimizing the disease-related deaths. The time interval $[0, T]$ of the simulation is chosen sufficiently large, such that the results are practically independent from the chosen final time T , see Table 1.



From the augmented index functional [21]

$$\bar{J}[u] = \varphi(\mathbf{x}(T)) + \int_0^T dt (\mathcal{C}(u(t)) + \lambda(t) \cdot (\mathbf{F}(\mathbf{x}(t), u(t)) - \dot{\mathbf{x}}(t))),$$

where $\mathbf{x} = (S, E, I, H, C, R, D)$ is the state vector, $\dot{\mathbf{x}} = \mathbf{F}(\mathbf{x}, u)$ is the dynamical system (1a)–(1g) and $\lambda(t)$ is a vector of time-dependent Lagrange multipliers (also denoted as *co-state variables*) $\lambda = (\lambda_S, \lambda_E, \lambda_I, \lambda_H, \lambda_C, \lambda_R, \lambda_D)$, one obtains the Hamiltonian function

$$\mathcal{H}(\mathbf{x}, u, \lambda) = \mathcal{C}(u) + \lambda \cdot \mathbf{F}(\mathbf{x}, u). \tag{9}$$

Following Pontryagin’s maximum principle [21, 22], the optimality condition reads

$$\frac{\partial \mathcal{H}}{\partial u} = 0 \Leftrightarrow u = \exp\left(\beta(\lambda_S - \lambda_E) \frac{IS}{N}\right). \tag{10}$$

Finally, the co-state equations and the final time conditions are obtained as

$$\dot{\lambda}(t) = -\nabla_{\mathbf{x}} \mathcal{H}, \tag{11}$$

$$\lambda(T) = \nabla_{\mathbf{x}} \varphi(\mathbf{x})|_T. \tag{12}$$

Together with the initial conditions $\mathbf{x}(0)$, the system (1a)–(1g), (11)–(12) represents a non-linear two-point boundary value problem. The full set of equations is given in Appendix D. Numerical solutions are obtained by using Matlab’s built-in routine `bvp4c` [60] in combination with an analytic Jacobian matrix and a step-size adaptive homotopy method, where the control parameter \mathcal{P} is gradually ramped up while always using the result of the previous step as initialization. The procedure is initiated from the numerical solution of the initial value problem (1a)–(1g) without interventions, see Fig. 2.

4 Results

4.1 Structure of the optimal intervention strategy

With optimal control of the transmission rate (in the sense of Sect. 3) via accordingly steered NPIs, the epidemic develops dramatically different from the uncontrolled case. The whole intervention is shown in Fig. 4 and can be structured into three phases:

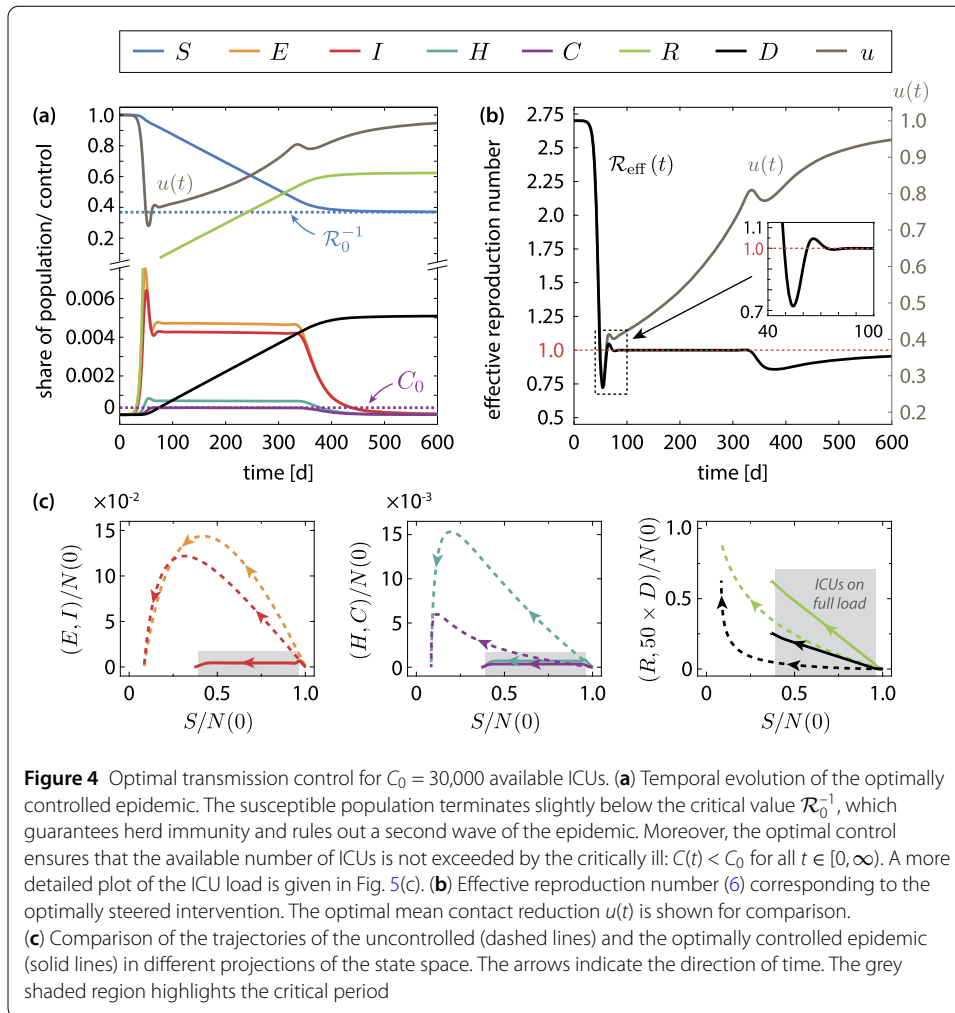
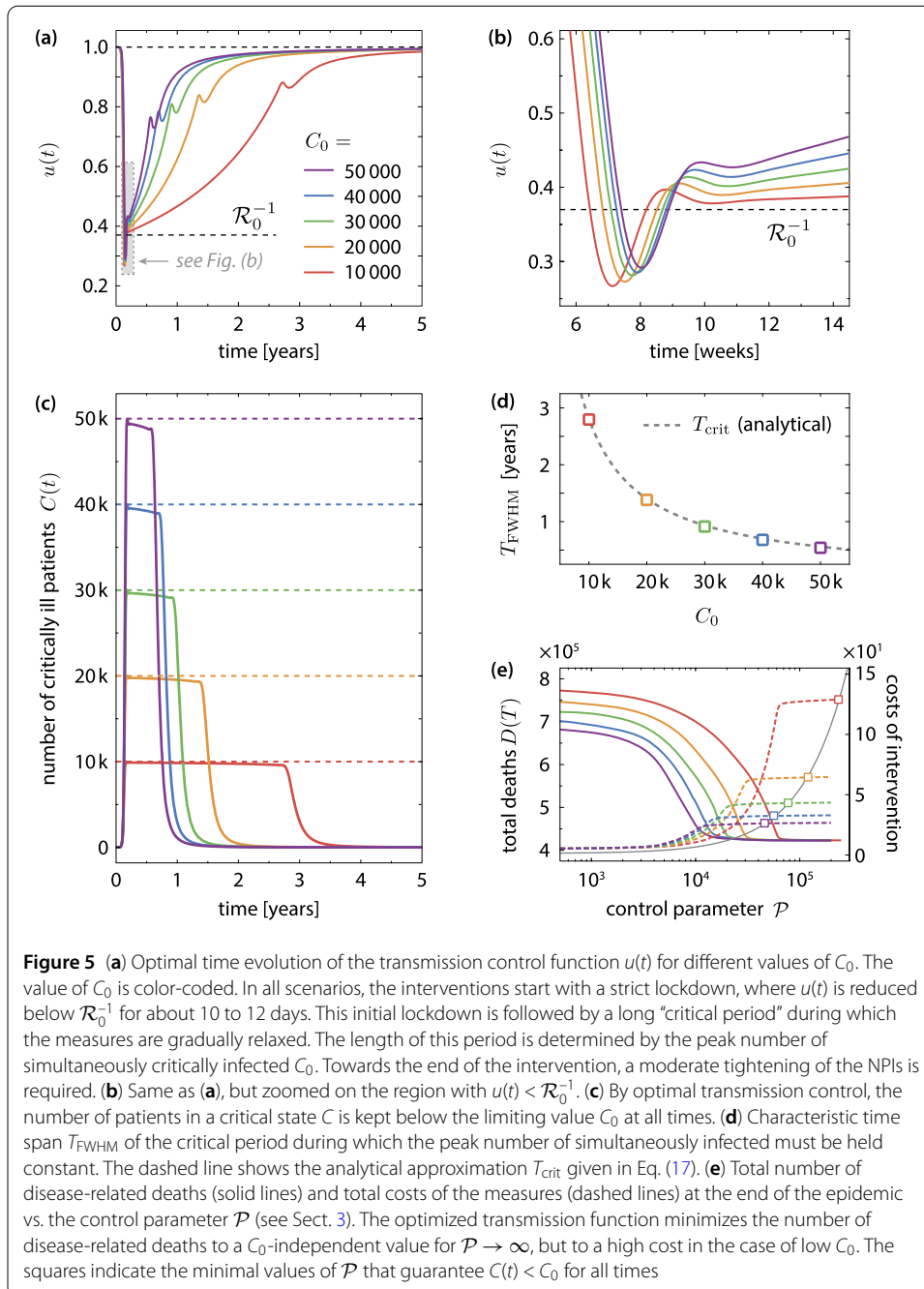


Figure 4 Optimal transmission control for $C_0 = 30,000$ available ICUs. **(a)** Temporal evolution of the optimally controlled epidemic. The susceptible population terminates slightly below the critical value \mathcal{R}_0^{-1} , which guarantees herd immunity and rules out a second wave of the epidemic. Moreover, the optimal control ensures that the available number of ICUs is not exceeded by the critically ill: $C(t) < C_0$ for all $t \in [0, \infty)$. A more detailed plot of the ICU load is given in Fig. 5(c). **(b)** Effective reproduction number (6) corresponding to the optimally steered intervention. The optimal mean contact reduction $u(t)$ is shown for comparison. **(c)** Comparison of the trajectories of the uncontrolled (dashed lines) and the optimally controlled epidemic (solid lines) in different projections of the state space. The arrows indicate the direction of time. The grey shaded region highlights the critical period

1. The intervention begins with a strict initial “lockdown” that is built up over a period of about 25 days (starting around day 25), see Fig. 4(a), (b). The effective reproduction number (6) must be held below one $\mathcal{R}_{\text{eff}} < 1$ for about 13 days, see Fig. 4(b) and Fig. 5(b). This strict initial intervention breaks the early exponential growth and damps the peak number of infected such that an overshoot of the critically ill population beyond C_0 is just barely avoided, see Fig. 4(a) and Fig. 5(c).
2. The initial lockdown is followed by a long period (about 300 days in the case of $C_0 = 30,000$), which is denoted as the “critical period” in the following, during which the number of simultaneously active cases is kept approximately constant. This corresponds to an effective reproduction number $\mathcal{R}_{\text{eff}} \approx 1$, see Fig. 4(b). During this phase, the intensive care system is constantly stressed by slightly less than C_0 patients in a critical state. This situation must of course be avoided in reality by all means, in particular, since stochastic fluctuations of the case number are not included in the deterministic model (1a)–(1g) at all. During this period, the NPIs are relaxed on a gradually increasing rate, but initially (when the disease is not yet widespread in the population) only very slowly, see Fig. 4(b). The duration of the critical period scales with C_0^{-1} . Further details are discussed in Sect. 4.3 below.



3. After the critical period, i.e., when the number of active cases starts to decay, a final moderate tightening of the measures is required. This is reflected by a notable dip in the transmission control function and a reduction of the effective reproduction number below one, see Fig. 4(b). This final intervention reflects the requirement to meet the herd immunity threshold towards the end of the intervention. An unnecessarily wide overshooting into the stable regime would result in additional infections and deaths, see Sect. 4.4. Finally, the measures are lifted on a gradually decreasing rate while the system slowly approaches the herd immunity threshold.

Figure 4(c) shows the trajectories of the controlled and the uncontrolled epidemic in different state space projections. By controlling the transmission of infection, the enormous excursion of the trajectory is prevented and the optimal path to a stable disease-free stationary state is taken. Note that the uncontrolled epidemic terminates far in the stable regime ($S(T)/N(T) \ll \mathcal{R}_0^{-1}$), whereas in the optimally controlled case the final state is just slightly below the stability threshold $S(T)/N(T) \lesssim \mathcal{R}_0^{-1}$.

We point out that the optimal transmission control described above differs from the results obtained for similar optimization problems considered in Refs. [43, 44, 47], which do not exhibit the distinct structural features of the intervention (initial lockdown, critical period, final phase intervention) presented here. A comparable result was described in Ref. [48], where the intervention was divided into four different phases which essentially coincide with our findings. Merely the lockdown was further subdivided into a “quick activation of a strong lockdown” and a “light lockdown release.”

4.2 Dependence on the maximum number of simultaneously critical cases

The state-dependent mortality rate (4a)–(4b) effectively imposes a state-constraint that strictly enforces $C < C_0$ for $\mathcal{P} \rightarrow \infty$, i.e., a maximum number of simultaneously infected in a critical condition. In principle, this allows to investigate the optimal control of other (less extreme) scenarios, where the maximum number of simultaneously critically infected should be held far below the number of available ICUs (i.e., the meaning of C_0 will be reinterpreted). In this case, the increased mortality rate f_1 is an artificial parameter that penalizes the excess of the critically infected population over a freely chosen threshold of C_0 . By ramping up the control parameter \mathcal{P} , an optimal solution with $C(t) < C_0$ for all $t \in [0, \infty)$ is found, that is independent of f_1 .

Figure 5 shows the optimal control for different values of C_0 . The time course of the optimally controlled transmission rate is qualitatively the same for all considered values of C_0 , see Fig. 5(a), (b). Most notably, the time scale of the entire intervention scenario is governed by the duration of the critical period, during which the number of critical patients is held at $C \lesssim C_0$, see Fig. 5(c). We characterize this time scale by the full width half maximum (FWHM) time $T_{\text{FWHM}} = t_2 - t_1$, where t_1 and $t_2 > t_1$ are the two points in time at which the number of critically infected equals half the allowed maximum value: $C(t_1) = C(t_2) = C_0/2$. As shown in Fig. 5(d), the FWHM time scales inversely with the peak number of simultaneously infected in a critical state: $T_{\text{FWHM}} \sim C_0^{-1}$. The minimization of the disease-related deaths is controlled by the parameter \mathcal{P} in the terminal cost function (7b). Figure 5(e) displays the progression of the optimization routine into the targeted optimal state (i.e., without excess of C_0) while \mathcal{P} is ramped up. At a certain value of \mathcal{P} , which depends on C_0 , the routine reaches a plateau where both the number of disease-related deaths as well as the total costs of the intervention measures $\int_0^T dt \mathcal{C}(u(t))$ become constant. The corresponding values of \mathcal{P} , which correspond to the scenario that fully avoids excess of critically ill over C_0 , are located on that plateau and are marked by square symbols in Fig. 5(e). The optimized transmission function minimizes the number of disease-related deaths to a C_0 -independent value $D_{\min}(T)$ for $\mathcal{P} \rightarrow \infty$, but at total cost that scales with C_0^{-1} . An analytical estimate of the minimum attainable number of deaths is given in Eq. (18).

Within the present model, further reduction of disease-related deaths below $D_{\min}(T)$ can only be achieved by pharmaceutical interventions, in particular by vaccination. The result of the C_0 -independent number of deaths at the end of the epidemic is an artifact

of the simplified modeling framework, in which a homogeneous population with an averaged set of parameters is considered. Since the mortality rate typically strongly depends on age and health condition, it might be advisable to extend the model and divide the compartments into several age or risk groups as in Refs. [11, 45, 54, 61]. The so-extended model features a matrix-valued transmission rate, which describes the infections caused by contacts within and between different groups, that could be further optimized by intra- and intergroup-specific measures. This is, however, beyond the scope of this paper.

4.3 Analysis of the critical period

The numerical results shown in Fig. 4(a), (b) indicate that during the critical period the populations $S, R,$ and D change approximately linear, while the active cases (E, I, H, C) are practically constant. To gain further insights, we consider the ansatz (for $t > t^*$)

$$S(t) \approx N(0) - \gamma_S(t - t^*), \quad R(t) \approx \gamma_R(t - t^*), \quad D(t) \approx \gamma_D(t - t^*),$$

where t^* is a reference time that depends on the initial conditions, $\gamma_S, \gamma_R, \gamma_D$ are initially unknown rates and the infected sub-populations $(E, I, H, C) \approx (E^*, I^*, H^*, C_0)$ are constant. From substituting the ansatz into the model equations (1a)–(1g), one obtains by a straightforward calculation analytical expressions for the rates

$$\gamma_S = \frac{1 - c(1 - f_0)}{(1 - m)c} \gamma_c C_0, \quad \gamma_R = \frac{1 - c(1 - mf_0)}{(1 - m)c} \gamma_c C_0, \quad \gamma_D = f_0 \gamma_c C_0,$$

and the constants

$$E^* \approx \frac{1}{\gamma_i} \gamma_S, \quad I^* \approx \frac{1}{\gamma_i} \gamma_S, \quad H^* \approx \frac{1}{\gamma_h} \frac{1}{cf_0} \gamma_D.$$

The rate of new infections per day γ_S during the critical period depends only on the parameters of the disease and the maximum capacity C_0 . Note that it holds $\gamma_S = \gamma_R + \gamma_D$, i.e., the number of active cases remains constant since susceptibles become infected at the same rate on which active cases either recover or die. The number of active cases in this *dynamical equilibrium* is a multiple of C_0 :

$$N_{act}^* = E^* + I^* + H^* + C^* = \left(\frac{1 - c(1 - f_0)}{c(1 - m)} \left(\frac{1}{\gamma_i} + \frac{1}{\gamma_i} \right) \gamma_c + \frac{1}{c} \frac{\gamma_c}{\gamma_h} + 1 \right) C_0.$$

With the parameters listed in Table 1, we find $N_{act}^* \approx 28.3C_0$, i.e., one out of about thirty infections turns critical.

Let us now come to the major results of this section. The ansatz stated above yields an instantaneous relationship between the current value of the transmission control function and the share of the susceptibles on the total population $S(t)/N(t)$, which is

$$u(t) \approx \frac{1}{\mathcal{R}_0} \frac{N(t)}{S(t)} \approx \frac{1}{\mathcal{R}_0} \left(1 - \frac{\gamma_S}{N(0)} (t - t^*) \right)^{-1} = \left(\mathcal{R}_0 - (\mathcal{R}_0 - 1) \frac{t - t^*}{T_{crit}} \right)^{-1} \tag{13}$$

for a certain range of t in $t^* < t < T_{crit}$ with T_{crit} defined below. Here, we approximated $N(t) \approx N(0)$ (since $\gamma_D \ll \gamma_S$). Note that Eq. (13) implies $\mathcal{R}_{eff} \approx 1$ during the critical period.

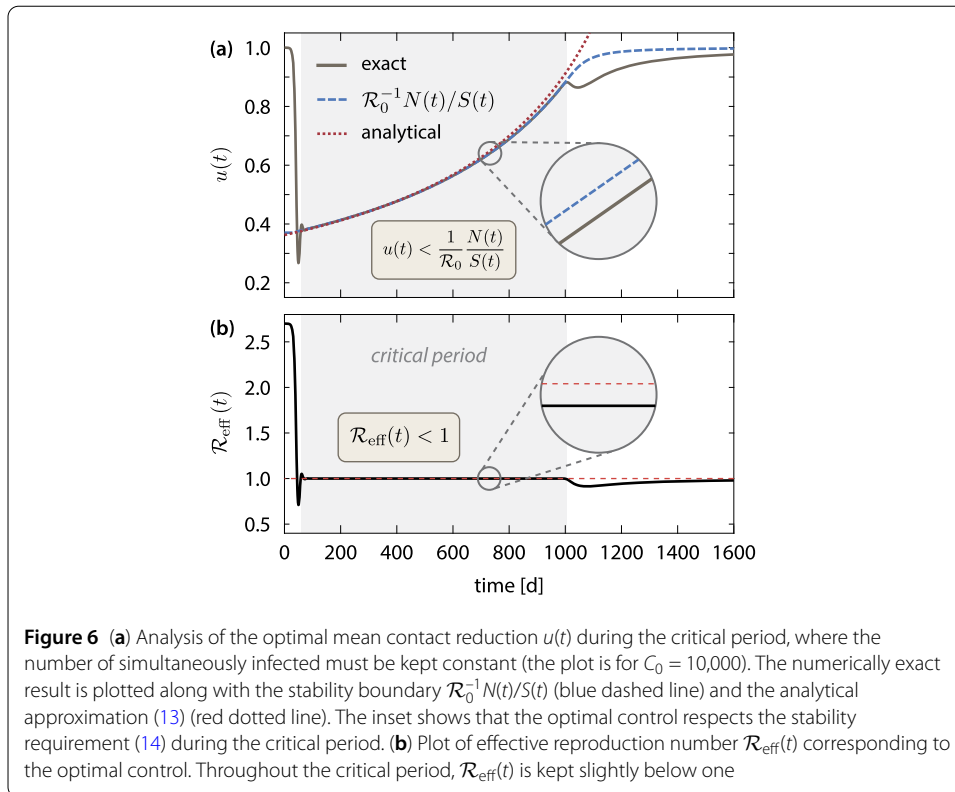


Figure 6 (a) Analysis of the optimal mean contact reduction $u(t)$ during the critical period, where the number of simultaneously infected must be kept constant (the plot is for $C_0 = 10,000$). The numerically exact result is plotted along with the stability boundary $\mathcal{R}_0^{-1}N(t)/S(t)$ (blue dashed line) and the analytical approximation (13) (red dotted line). The inset shows that the optimal control respects the stability requirement (14) during the critical period. (b) Plot of effective reproduction number $\mathcal{R}_{\text{eff}}(t)$ corresponding to the optimal control. Throughout the critical period, $\mathcal{R}_{\text{eff}}(t)$ is kept slightly below one

This approximate relation is an interesting result, as it hints that the obtained optimal control steers the system’s trajectory close to the stability boundary. Comparison with the stability criterion for the disease-free stationary state $\mathcal{R}_0 < \bar{N}/\bar{S}$, see Eq. (19), suggests that during the critical period one must make sure that $\mathcal{R}_{\text{eff}}(t) < 1$, i.e.,

$$u(t) < \frac{1}{\mathcal{R}_0} \frac{N(t)}{S(t)}. \tag{14}$$

This allows to have a stable control of the number of active cases, while the intervention measures can be gradually relaxed. Stable means that sufficiently small fluctuations of the number of infected are damped and do not lead to a new exponential outbreak of the epidemic. Indeed, substituting $u(t) = (1 + \varepsilon)N(t)/(\mathcal{R}_0S(t))$ into the model equations (1a)–(1g) yields a linear, autonomous dynamical system (up to the state-dependent mortality rate (4a)–(4b)), which is easily seen to evolve close to a stable dynamical equilibrium for $\varepsilon < 0$ and $|\varepsilon| \ll 1$, see Appendix B. The optimal transmission control function is shown in Fig. 6 along with the analytical approximation (13), the stability criterion (14) and the corresponding effective reproduction number for the critical period.

We formulate the stability criterion (14) once again in a different way. Since it holds $S(t) \approx N(0) - N_{\text{cases}}(t)$, where $N_{\text{cases}}(t)$ is the cumulative number of cases that includes next to the active cases also the recovered and deceased population $N_{\text{cases}}(t) = N_{\text{act}}(t) + R(t) + D(t)$, the stability criterion (14) can be written as

$$u(t) < \frac{1}{\mathcal{R}_0} \left(1 - \frac{N_{\text{cases}}(t)}{N(0)} \right)^{-1}. \tag{15}$$

Hence, since the optimal control depends solely on the cumulative number of cases, it is crucial to have an accurate estimate of N_{cases} at any time during the critical period. Next, we derive an upper limit for the admissible rate of change of $u(t)$. By differentiating Eq. (14), using Eq. (1a) and approximating $N(t) \approx N(0)$ as well as $I(t) \approx I^*$ (see above), we obtain

$$\dot{u}(t) < \frac{1}{\mathcal{R}_0} \left(-\frac{\dot{D}(t)}{S(t)} - \frac{N(t)}{S^2(t)} \dot{S}(t) \right) < \frac{N(t)}{S(t)} u(t) \frac{\gamma_i I(t)}{N(t)} < \left(\frac{N(t)}{\mathcal{R}_0 S(t)} \right)^2 \frac{\mathcal{R}_0 \gamma_S}{N(0)}.$$

Using the approximation (13), the rate on which the measures can be relaxed is limited by the square of the current value of the control function. It holds

$$\dot{u}(t) < \frac{\mathcal{R}_0 \gamma_S}{N(0)} u^2(t). \tag{16}$$

The numerically computed optimal control obeys the criteria (15)–(16), see Fig. 6, and is therefore (weakly) stable against small perturbations. The merely weak stability reflects the demand for minimal socio-economic costs, see Sect. 3. The two rules (15)–(16) for the optimal and stable steering of the transmission control function are widely independent of the details of the current model system. Equivalent results for a stable dynamical equilibrium with a constant number of infected cases are easily obtained for the much simpler SIR model.

The characteristic duration T_{crit} of the critical period is estimated from Eq. (13) and the condition $u(t^* + T_{\text{crit}}) \approx 1$. One obtains

$$T_{\text{crit}} \approx \frac{N(0)}{\gamma_S} \left(1 - \frac{1}{\mathcal{R}_0} \right) \propto \frac{N(0)}{C_0} \left(1 - \frac{1}{\mathcal{R}_0} \right), \tag{17}$$

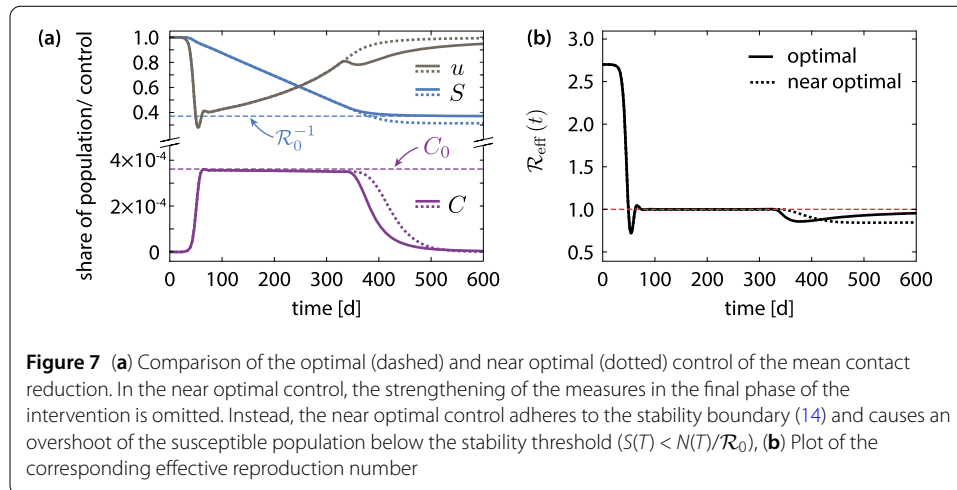
which is in excellent agreement with the numerically obtained values for the FWHM time plotted in Fig. 5(d). Finally, we estimate of the total number of disease-related deaths from $D(T) \approx D(t^* + T_{\text{crit}}) \approx \gamma_D T_{\text{crit}}$ as

$$D(T) \approx N(0) \frac{\gamma_D}{\gamma_S} \left(1 - \frac{1}{\mathcal{R}_0} \right) = N(0) \frac{(1-m)c f_0}{1-c(1-f_0)} \left(1 - \frac{1}{\mathcal{R}_0} \right), \tag{18}$$

which is independent of C_0 , cf. Sect. 4.2 and Fig. 5(e).

4.4 Final phase of the intervention

Finally, we briefly discuss the moderate tightening of the measures in the last (third) phase of the intervention. To this end, we compare the optimal intervention scenario with a nearly optimal control, which lacks the last intervention phase as shown in Fig. 7. In the case of nearly optimal control, the mean contact reduction after the initial lockdown continuously follows the course of the stability boundary (14), which leads to an excess of infections beyond the required herd immunity threshold, see Fig. 7(a). The final state therefore is considerably further in the stable region than required. This implies that more infections than necessary are passed through, which results in exceeding the minimum number of deaths (not shown), cf. Eq. (18). In order to prevent this, the measures must be slightly tightened towards the end of the intervention such that the number of active cases is diminished and thus an unnecessary decrease of the susceptible population below the herd immunity threshold is avoided.



5 Summary and conclusions

Non-pharmaceutical measures to control the spread of infectious diseases and to prevent a potential collapse of the health care system must be precisely coordinated in terms of timing and intensity. Based on well-calibrated mathematical models, the optimal intervention strategy for specific scenarios and objectives can be computed using continuous-time optimal control theory.

In this paper, an extended SEIR model was calibrated to reproduce the data of the initial exponential growth phase of the COVID-19 pandemic in Germany. Optimal control theory has been applied for the scenario in which an effective vaccine is impossible or will never be found and the epidemic must be controlled with purely non-pharmaceutical measures. We have computed the optimal control of the transmission rate that satisfies competing objectives: First, the minimization of the disease-related deaths by strictly avoiding an overflow of intensive care resources and, second, the suppression of a second outbreak by establishing sufficient natural immunity at the end of the measures. Moreover, the total costs of the intervention shall be kept at a necessary minimum for socio-economic reasons.

The optimal control obtained in this paper is a single-intervention scenario that exhibits several notable features, which allow to structure the whole intervention into three distinct phases: (i) strict initial lockdown, (ii) critical period and (iii) moderate tightening of measures in the final phase. The obtained control differs from the results described in related works [43, 44, 47], but is comparable to the NPI strategy presented in Ref. [48]. We have shown that our optimized time-resolved NPI policy is robust under parameter variation and developed a qualitative understanding of its distinct phases.

The comparison of the computed optimal transmission control function with the stability criteria (15)–(16) reveals, however, that the obtained solution is in fact a tightrope walk close to the stability boundary of the system, where socio-economic costs and the risk of a new outbreak must be constantly balanced against one another. Furthermore, our analysis clearly shows that the goal of achieving herd immunity via natural infections is either extremely expensive (in terms of socio-economic costs due to measures maintained over a long period of time) or extremely dangerous (due to the constantly high load on intensive care resources just below the stability limit). Note that the values of C_0 considered in the computations are relatively high throughout. In any case, in view of the long duration and

the enormous number of infections that this route entails, as well as the uncertain role of sequelae and the uncertain prospects for appropriate vaccines, it is strongly advisable to consider other strategies, in particular the attempt to reduce the number of cases to a level that is manageable for case tracking [62] or to eradicate the epidemic completely [63].

Appendix A: Stability analysis of the disease-free stationary state

Without intervention, i.e. $u = 1$, the system (1a)–(1g) has a family of disease-free stationary states $\bar{x} = (\bar{S}, 0, 0, 0, 0, \bar{R}, \bar{D})$. The stability of a stationary state with respect to small perturbations $\bar{x} \rightarrow \bar{x} + \delta x(t)$ is determined by the sign of the real parts of the eigenvalues η of the linearized system’s coefficient matrix

$$A(\bar{x}) = \begin{pmatrix} 0 & 0 & -\beta\bar{S}/\bar{N} & 0 & 0 & 0 & 0 \\ 0 & -\gamma_l & \beta\bar{S}/\bar{N} & 0 & 0 & 0 & 0 \\ 0 & \gamma_l & -\gamma_i & 0 & 0 & 0 & 0 \\ 0 & 0 & (1-m)\gamma_i & -\gamma_h & (1-f_0)\gamma_c & 0 & 0 \\ 0 & 0 & 0 & c\gamma_h & -\gamma_c & 0 & 0 \\ 0 & 0 & m\gamma_i & (1-c)\gamma_h & 0 & 0 & 0 \\ 0 & 0 & 0 & 0 & f_0\gamma_c & 0 & 0 \end{pmatrix}.$$

with $\bar{N} = \bar{S} + \bar{R}$. From the characteristic polynomial

$$0 = \chi(\eta) = \det(A(\bar{x}) - \eta I),$$

one obtains the eigenvalues

$$\eta_{\pm}^{(1)} = \frac{1}{2}(-(\gamma_i + \gamma_l) \pm \sqrt{(\gamma_i - \gamma_l)^2 + 4\mathcal{R}_0\gamma_i\gamma_l\bar{S}/\bar{N}}),$$

$$\eta_{\pm}^{(2)} = \frac{1}{2}(-(\gamma_c + \gamma_h) \pm \sqrt{(\gamma_c - \gamma_h)^2 + 4c(1-f_0)\gamma_c\gamma_h}),$$

and the threefold degenerate eigenvalue $\eta^{(0)} = 0$. Since $c(1-f_0) < 1$, it holds $\eta_{\pm}^{(2)} < 0$. The leading eigenvalue is $\eta_+^{(1)}$, which is negative for

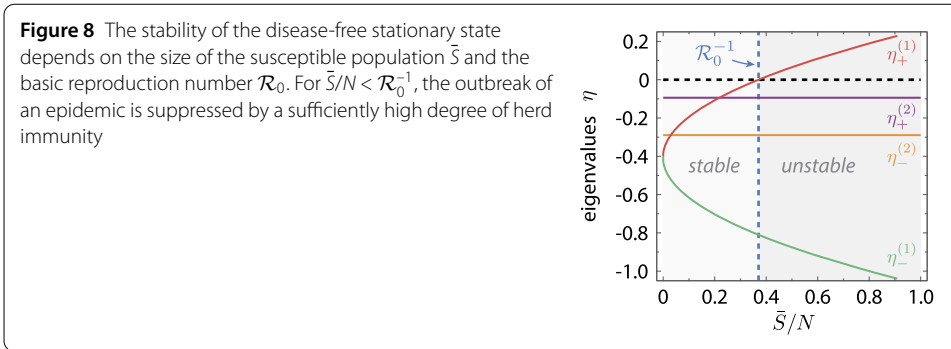
$$\bar{S}/\bar{N} < \mathcal{R}_0^{-1}, \tag{19}$$

see Fig. 8. Hence, the disease-free stationary state is unstable if the susceptible population size exceeds a critical threshold value that is given by the inverse basic reproduction number (5). For $\bar{S}/\bar{N} < \mathcal{R}_0^{-1}$ an epidemic outbreak is suppressed by a sufficiently high degree of herd immunity.

Appendix B: Dynamical equilibrium and stability during the critical period

For the stability analysis of the dynamical equilibrium during the critical period it is sufficient to consider the (S, E, I) -block of the system (1a)–(1g), which drives the remaining equations. At first,

$$\dot{S} = -\beta u(t) \frac{IS}{N}, \quad \dot{E} = \beta u(t) \frac{IS}{N} - \gamma_l E, \quad \dot{I} = \gamma_l E - \gamma_i I,$$



is a nonlinear and non-autonomous dynamical system. Substituting the control function

$$u(t) = (1 + \varepsilon) \frac{1}{\mathcal{R}_0} \frac{N(t)}{S(t)},$$

yields a linear and autonomous system

$$\dot{S} = -(1 + \varepsilon)\gamma_i I, \quad \dot{E} = (1 + \varepsilon)\gamma_i I - \gamma_l E, \quad \dot{I} = \gamma_l E - \gamma_i I.$$

For $\varepsilon = 0$, it is easily seen that $\dot{E} + \dot{I} = 0$, such that there exists a dynamical equilibrium with a constant number of actively infected: $E^* + I^* = \text{const.}$, where $E^* = (1 + \gamma_i/\gamma_l)I^*$. The corresponding susceptible population is linearly decreasing on a rate $\gamma_S = \gamma_i I^*$. The stability of the dynamical equilibrium (E^*, I^*) is determined by the roots of the characteristic polynomial

$$0 = \Lambda^2 + (\gamma_l + \gamma_i)\Lambda - \gamma_l \gamma_i \varepsilon$$

that are obtained as

$$\Lambda_{\pm} = -\frac{\gamma_l + \gamma_i}{2} \pm \sqrt{\left(\frac{\gamma_l + \gamma_i}{2}\right)^2 + \gamma_l \gamma_i \varepsilon}.$$

Clearly, for $\varepsilon > 0$, the dynamical equilibrium becomes unstable due to $\Lambda_+ > 0$. The stability boundary is given by $\varepsilon = 0$, on which the dynamical equilibrium exists. The optimal control obtained in the main text drives the system slightly below the stability boundary ($\varepsilon < 0$, $|\varepsilon| \ll 1$), see Fig. 6(a). In this case it holds $\Lambda_{\pm} < 0$, such that the system is weakly stable against small perturbations, because the number of active cases is constantly decreasing.

Appendix C: Parameter adjustment

The parameters are adjusted such that the model reproduces the data of the early exponential growth phase of the COVID-19 pandemic in Germany. It is of course questionable to calibrate an epidemic model to a single country, but in a scenario with extensive border closures this seems to be justified. In the exponential growth phase of the epidemic, all sub-populations grow exponentially with the same rate, see Fig. 2(b). This observation can be exploited to derive a series of algebraic equations (which hold approximately in the initial phase of the epidemic) that relate all state variables to each other. On the basis of

empirical data (reported number of cases and deaths etc.), several missing model parameters can be directly determined from the algebraic relations. The number of reported cases and deaths used in this study is based on the figures provided by the Robert Koch-Institute [64, 65].

One starts with the ansatz

$$I(t) \approx I(0)e^{\Gamma t}, \quad S(t) \approx N(0), \tag{20}$$

where Γ is the initial exponential growth rate that is estimated from reported data (see Fig. 2(b)) as $\Gamma \approx 0.26d^{-1}$ (doubling time of infections within $\Gamma^{-1} \log(2) \approx 2.67d$). Substituting Eq. (20) in Eqs. (1b)–(1c) yields

$$E(t) \approx \frac{1}{\gamma_i}(\Gamma + \gamma_i)I(t)$$

and the relation between the growth rate and \mathcal{R}_0 :

$$\left(1 + \frac{\Gamma}{\gamma_i}\right)\left(1 + \frac{\Gamma}{\gamma_i}\right) = \mathcal{R}_0. \tag{21}$$

Note that Eq. (21) is equivalent to the equation for the leading eigenvalue $\eta_+^{(1)}$ if the whole population is susceptible, i.e. $\Gamma = \eta_+^{(1)}|_{\bar{S}=N(0)}$ (see Appendix A). Hence, Eq. (21) implies that the exponential growth rate Γ changes sign at $\mathcal{R}_0 = 1$, i.e., the epidemic recedes for $\mathcal{R}_0 < 1$. The mean incubation period was reported to be 5.1d, but there are indications that the latency time may be shorter [66]. Assuming the onset of infectiousness 2.5d before the onset of symptoms, this implies an average latency period of $\gamma_i^{-1} = 2.6d$, i.e., the latency period is assumed to equal roughly half of the incubation period. The reported values of the basic reproduction number \mathcal{R}_0 are heavily scattered. According to the Robert Koch Institute, serious estimates range between 2.4 and 3.3 [67]. In the following $\mathcal{R}_0 = 2.7$ shall be used, which is situated approximately in the middle of the interval in question. From Eq. (21), the corresponding average infectious period is obtained as $\gamma_i^{-1} \approx 2.35d$.

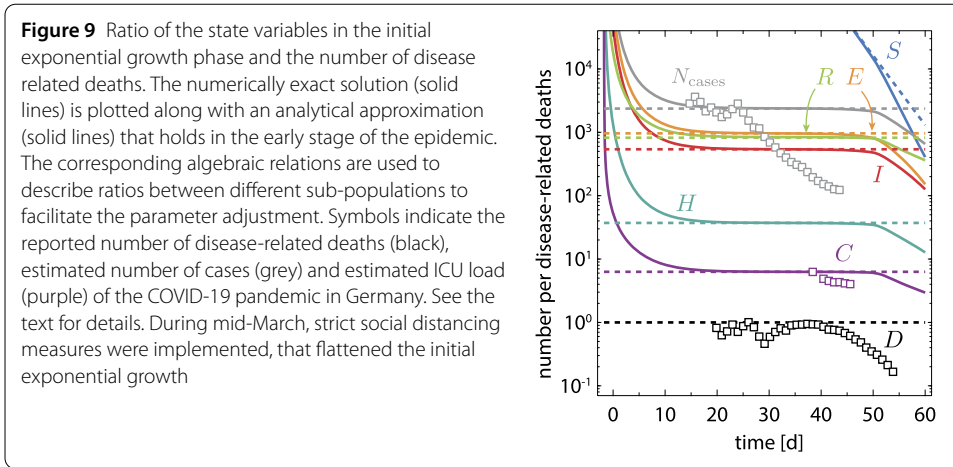
The overall infection fatality rate of COVID-19 was estimated as 0.66% [68], such that $(1 - m)cf_0 = 0.0066$. On April 8, the Robert Koch Institute reported that a fraction of $f_0 = 0.31$ patients in a critical state died (without ICU overflow) [69]. Finally, the fraction of infected with at most mild symptoms is estimated as $m = 0.92$, such that $c = 0.0213/(1 - m) \approx 0.266$.

Substituting the exponential ansatz (20) in Eqs. (1d)–(1g), yields

$$\begin{aligned} H(t) &\approx \frac{(1 - m)}{K} \frac{\gamma_i}{\Gamma} \left(1 + \frac{\gamma_c}{\Gamma}\right) I(t), & C(t) &\approx \frac{(1 - m)c}{K} \frac{\gamma_i \gamma_h}{\Gamma^2} I(t), \\ R(t) &\approx \frac{\gamma_i}{\Gamma} \left(m + \frac{(1 - m)(1 - c)}{K} \frac{\gamma_h}{\Gamma} \left(1 + \frac{\gamma_c}{\Gamma}\right)\right) I(t), & D(t) &\approx \frac{(1 - m)cf_0}{K} \frac{\gamma_i \gamma_c \gamma_h}{\Gamma^3} I(t) \end{aligned}$$

with $K = 1 + (\gamma_h + \gamma_c)/\Gamma + \gamma_c \gamma_h (1 - (1 - f_0)c)/\Gamma^2$. The analytically obtained ratio between all sub-population and deaths (which are believed to be the most reliably reported data) are plotted along with the corresponding numerically exact result for the initial uncontrolled epidemic in Fig. 9(b). The analytical results imply the relation

$$D(t)/C(t) = \gamma_c f_0 / \Gamma. \tag{22}$$



Unfortunately, there is only little data available on the demand for ICUs in the early phase of the epidemic. In mid-March 2020, i.e. near the end of the initial exponential growth phase, the German Interdisciplinary Association for Intensive Care and Emergency Medicine (DIVI) initiated a register that reports on the availability of ICUs in Germany [70]. On March 27, 687 out of 1160 hospitals with ICUs contributed to the register and reported a total number of 939 COVID-19 patients in a critical state receiving intensive care [71]. At the same day, 253 disease-related deaths were reported. From the estimated ratio $C/D \approx 6.3$ (the actual number of critical patients was estimated based on the ratio of contributing and non-contributing hospitals as $C \approx 1586$), the average period after which patients in a critical state either recover or die, is estimated from Eq. (22) as $\gamma_c^{-1} \approx 7.5\text{d}$.

Finally, assuming that only $r = 2/3$ of all cases have been discovered initially and an assumed average time delay between infection and report of cases of $\Delta t_r = 5\text{d}$, the number of actual cases is estimated from the number of reported cases as $N_{\text{cases}}^{\text{est}}(t) = r^{-1}N_{\text{cases}}^{\text{rep}}(t + \Delta t_r) = r^{-1}e^{\Gamma\Delta t_r}N_{\text{cases}}^{\text{rep}}(t) \approx 5.5N_{\text{cases}}^{\text{rep}}(t)$. This yields a good agreement between the simulated number of cases ($N_{\text{cases}} = E + I + H + C + R + D$) and $N_{\text{cases}}^{\text{est}}$ before measures came into force, see Fig. 2(a) and Fig. 9. The average time between infection and death Δt_d can be estimated from the ratio $N_{\text{cases}}^{\text{est}}(t)/D(t) \approx 2370$ (see Fig. 8(b)) and $N_{\text{cases}}^{\text{est}}(t - \Delta t_d) = N_{\text{cases}}^{\text{est}}(t)e^{-\Gamma\Delta t_d} = D(t)$ as $\Delta t_d \approx 29.9\text{d}$.

Appendix D: Two-point boundary value problem

Rescaling the populations $\mathbf{x} = (S, E, I, H, C, R, D)$ subject to the dynamical system (1a)–(1g) by the initial population size $N(0)$ and using $N(t) = N(0) - D(t)$, see Eq. (3), we obtain the equations of motion for the rescaled sub-populations $\tilde{\mathbf{x}}(t) = \mathbf{x}(t)/N(0)$ as

$$\dot{\tilde{S}} = -\beta u(t) \frac{\tilde{I}\tilde{S}}{1 - \tilde{D}}, \tag{23a}$$

$$\dot{\tilde{E}} = \beta u(t) \frac{\tilde{I}\tilde{S}}{1 - \tilde{D}} - \gamma_i \tilde{E}, \tag{23b}$$

$$\dot{\tilde{I}} = \gamma_i \tilde{E} - \gamma_i \tilde{I}, \tag{23c}$$

$$\dot{\tilde{H}} = (1 - m)\gamma_i \tilde{I} + (1 - f(\tilde{C}/\tilde{C}_0))\gamma_c \tilde{C} - \gamma_h \tilde{H}, \tag{23d}$$

$$\dot{\tilde{C}} = c\gamma_h \tilde{H} - \gamma_c \tilde{C}, \quad (23e)$$

$$\dot{\tilde{R}} = m\gamma_i \tilde{I} + (1-c)\gamma_h \tilde{H}, \quad (23f)$$

$$\dot{\tilde{D}} = f(\tilde{C}/\tilde{C}_0)\gamma_c \tilde{C}, \quad (23g)$$

where $\tilde{C}_0 = C_0/N(0)$. The co-state equations of the optimal control problem considered in Sect. 3 for the rescaled Lagrange multipliers $\tilde{\lambda}(t) = N(0)\lambda(t)$ read

$$\begin{aligned} \dot{\tilde{\lambda}}_S(t) &= L + \beta(\tilde{\lambda}_S - \tilde{\lambda}_E)u \frac{\tilde{I}}{1 - \tilde{D}}, \\ \dot{\tilde{\lambda}}_E(t) &= L + \gamma_I(\tilde{\lambda}_E - \tilde{\lambda}_I), \\ \dot{\tilde{\lambda}}_I(t) &= L + \beta(\tilde{\lambda}_S - \tilde{\lambda}_E)u \frac{\tilde{S}}{1 - \tilde{D}} + \gamma_I(\tilde{\lambda}_I - \tilde{\lambda}_H + m(\tilde{\lambda}_H - \tilde{\lambda}_R)), \\ \dot{\tilde{\lambda}}_H(t) &= L + \gamma_h(\tilde{\lambda}_H - \tilde{\lambda}_R + c(\tilde{\lambda}_R - \tilde{\lambda}_C)), \\ \dot{\tilde{\lambda}}_C(t) &= L + \gamma_c(\tilde{\lambda}_C - \tilde{\lambda}_H) + \gamma_c \left(f\left(\frac{\tilde{C}}{\tilde{C}_0}\right) + \frac{\tilde{C}}{\tilde{C}_0} f'\left(\frac{\tilde{C}}{\tilde{C}_0}\right) \right) (\tilde{\lambda}_H - \tilde{\lambda}_D), \\ \dot{\tilde{\lambda}}_R(t) &= L, \\ \dot{\tilde{\lambda}}_D(t) &= 0, \end{aligned}$$

with

$$L = -\frac{u \log(u)}{1 - \tilde{D}}, \quad u = \exp\left(\beta(\tilde{\lambda}_S - \tilde{\lambda}_E) \frac{\tilde{I}\tilde{S}}{1 - \tilde{D}}\right).$$

The initial conditions are taken as

$$\tilde{S}(0) = 1 - \tilde{E}(0), \quad \tilde{E}(0) = 2.41 \times 10^{-7}, \quad \tilde{I}(0) = \tilde{H}(0) = \tilde{C}(0) = \tilde{R}(0) = \tilde{D}(0) = 0,$$

and the final time conditions (12) read

$$\begin{aligned} \tilde{\lambda}_S(T) &= -\frac{1}{\varepsilon} \frac{\mathcal{R}_0}{1 - \tilde{D}(T)} \left(1 - \frac{\tilde{S}(T)}{1 - \tilde{D}(T)}\right) \log\left(\frac{1}{\varepsilon} \left[1 - \frac{\mathcal{R}_0 \tilde{S}(T)}{1 - \tilde{D}(T)}\right]\right), \\ \tilde{\lambda}_{E,I,H,C,R}(T) &= \frac{1}{\varepsilon} \frac{\mathcal{R}_0}{1 - \tilde{D}(T)} \frac{\tilde{S}(T)}{1 - \tilde{D}(T)} \log\left(\frac{1}{\varepsilon} \left[1 - \frac{\mathcal{R}_0 \tilde{S}(T)}{1 - \tilde{D}(T)}\right]\right), \\ \tilde{\lambda}_D(T) &= N(0)\mathcal{P}. \end{aligned}$$

The choice of the initial time conditions guarantees $u(0) = 1$ (no intervention) at the beginning of the scenario.

Acknowledgements

Not applicable.

Funding

Open access funding provided by Projekt DEAL.

Abbreviations

COVID-19, coronavirus disease 2019; FWHM, full width half maximum; ICU, intensive care unit; NPI, non-pharmaceutical intervention; S(E)IR, susceptible-(exposed)-infectious-recovered.

Availability of data and materials

Data were taken from online resources as cited and described in detail in Appendix C. Matlab source codes can be made available upon request.

Competing interests

The authors declare that they have no competing interests.

Authors' contributions

MK initiated the research, implemented the numerical routines, performed the numerical and analytical calculations and prepared the figures. TK initiated the analysis that lead to the qualitative understanding of the optimal control and its stability during the "critical period". Both authors contributed to the interpretation of the results and wrote the manuscript. All authors read and approved the final manuscript.

Publisher's Note

Springer Nature remains neutral with regard to jurisdictional claims in published maps and institutional affiliations.

Received: 23 April 2020 Accepted: 6 August 2020 Published online: 18 August 2020

References

1. Zhu N, Zhang D, Wang W, Li X, Yang B, Song J, Zhao X, Huang B, Shi W, Lu R, Niu P, Zhan F, Ma X, Wang D, Xu W, Wu G, Gao GF, Tan W. A novel coronavirus from patients with pneumonia in China. *N Engl J Med*. 2020;382(8):727–33. <https://doi.org/10.1056/NEJMoa2001017>.
2. Wu F, Zhao S, Yu B et al. A new coronavirus associated with human respiratory disease in China. *Nature*. 2020;579:265–9. <https://doi.org/10.1038/s41586-020-2008-3>.
3. Phua J, Weng L, Ling L, Egi M, Lim CM, Divatia JV, Shrestha BR, Arabi YM, Ng J, Gomersall CD, Nishimura M, Koh Y, Du B. Intensive care management of coronavirus disease 2019 (COVID-19): challenges and recommendations. *Lancet Resp Med*. 2020. [https://doi.org/10.1016/s2213-2600\(20\)30161-2](https://doi.org/10.1016/s2213-2600(20)30161-2).
4. Ferguson NM, Laydon D, Nedjati-Gilani G et al. Impact of non-pharmaceutical interventions (NPIs) to reduce COVID-19 mortality and healthcare demand. Imperial College Lond (16-03-2020) (2020). <https://doi.org/10.25561/77482>.
5. Flaxman S, Mishra S, Gandy A, Unwin HJT, Mellan TA, Coupland H, Whittaker C, Zhu H, Berah T, Eaton JW, Monod M, Imperial College COVID-19 Response Team, Ghani AC, Donnelly CA, Riley SM, Vollmer MAC, Ferguson NM, Okell LC, Bhatt S. Estimating the effects of non-pharmaceutical interventions on COVID-19 in Europe. *Nature*. 2020. <https://doi.org/10.1038/s41586-020-2405-7>.
6. Chang SL, Harding N, Zachreson C, Cliff OM, Prokopenko M. Modelling transmission and control of the COVID-19 pandemic in Australia. 2020. [arXiv:2003.10218](https://arxiv.org/abs/2003.10218).
7. Ng KY, Gui MM. COVID-19: development of a robust mathematical model and simulation package with consideration for ageing population and time delay for control action and resusceptibility. *Phys D, Nonlinear Phenom*. 2020;411:132599. <https://doi.org/10.1016/j.physd.2020.132599>.
8. Bouchnita A, Jebrane A. A hybrid multi-scale model of COVID-19 transmission dynamics to assess the potential of non-pharmaceutical interventions. *Chaos Solitons Fractals*. 2020;138:109941. <https://doi.org/10.1016/j.chaos.2020.109941>.
9. Jia J, Ding J, Liu S, Liao G, Li J, Duan B, Wang G, Zhang R. Modeling the control of COVID-19: impact of policy interventions and meteorological factors. *Electron J Differ Equ*. 2020;23:1.
10. Kucharski AJ, Russell TW, Diamond C, Liu Y, Edmunds J, Funk S, Eggo RM, Sun F, Jit M, Munday JD, Davies N, Gimma A, van Zandvoort K, Gibbs H, Hellewell J, Jarvis CI, Clifford S, Quilty BJ, Bosse NI, Abbott S, Klepac P, Flasche S. Early dynamics of transmission and control of COVID-19: a mathematical modelling study. *Lancet Infect Dis*. 2020;20(5):553–8. [https://doi.org/10.1016/S1473-3099\(20\)30144-4](https://doi.org/10.1016/S1473-3099(20)30144-4).
11. Barbarossa MV, Fuhrmann J, Heidecke J, Vinod Varma H, Castelletti N, Meinke JH, Krieg S, Lippert T. A first study on the impact of current and future control measures on the spread of COVID-19 in Germany. *medRxiv* 2020. <https://doi.org/10.1101/2020.04.08.20056630>.
12. Kissler SM, Tedijanto C, Goldstein E, Grad YH, Lipsitch M. Projecting the transmission dynamics of SARS-CoV-2 through the postpandemic period. *Science*. 2020;368(6493):860–8. <https://doi.org/10.1126/science.abb5793>.
13. Sesterhenn JL. Adjoint-based data assimilation of an epidemiology model for the Covid-19 pandemic in 2020. 2020. [arXiv:2003.13071](https://arxiv.org/abs/2003.13071).
14. Khailaie S, Mitra T, Bandyopadhyay A, Schips M, Mascheroni P, Vanella P, Lange B, Binder S, Meyer-Hermann M. Estimate of the development of the epidemic reproduction number R_t from coronavirus SARS-CoV-2 case data and implications for political measures based on prognostics. *medRxiv* 2020. <https://doi.org/10.1101/2020.04.04.20053637>.
15. Engbert R, Rabe MM, Kliegl R, Reich S. Sequential data assimilation of the stochastic SEIR epidemic model for regional COVID-19 dynamics. *medRxiv* 2020. <https://doi.org/10.1101/2020.04.13.20063768>.
16. Dehning J, Zierenberg J, Spitzner FP, Wibral M, Neto JP, Wilczek M, Priesemann V. Inferring change points in the spread of COVID-19 reveals the effectiveness of interventions. *Science*. 2020. <https://doi.org/10.1126/science.abb9789>.
17. Brauner JM, Mindermann S, Sharma M, Stephenson AB, Gavenčič T, Johnston D, Salvatier J, Leech G, Besiroglu T, Altman G, Ge H, Mikulík V, Hartwick M, Teh YW, Chindelevitch L, Gal Y, Kulveit J. The effectiveness and perceived burden of nonpharmaceutical interventions against COVID-19 transmission: a modelling study with 41 countries. *medRxiv* 2020. <https://doi.org/10.1101/2020.05.28.20116129>.

18. Tsay C, Lejarza F, Stadtherr MA, Baldea M. Modeling, state estimation, and optimal control for the US COVID-19 outbreak. *Sci Rep*. 2020;10:10711. <https://doi.org/10.1038/s41598-020-67459-8>.
19. Tarrataca L, Dias CM, Haddad DB, Arruda EF. Flattening the curves: on-off lock-down strategies for COVID-19 with an application to Brazil. 2020. [arXiv:2004.06916](https://arxiv.org/abs/2004.06916).
20. Bin M, Cheung P, Crisostomi E, Ferraro P, Lhachemi H, Murray-Smith R, Myant C, Parisini T, Shorten R, Stein S, Stone L. On fast multi-shot COVID-19 interventions for post lock-down mitigation. 2020. [arXiv:2003.09930](https://arxiv.org/abs/2003.09930).
21. Lewis FL, Vrabie D, Syrmos VL. Optimal control. New York: Wiley; 2012. <https://doi.org/10.1002/9781118122631>.
22. Pontryagin LS, Boltyanskii VG, Gamkrelidze RV, Mishchenko EF. The mathematical theory of optimal processes. New York: Wiley; 1962.
23. Wickwire K. Mathematical models for the control of pests and infectious diseases: a survey. *Theor Popul Biol*. 1977;11(2):182–238. [https://doi.org/10.1016/0040-5809\(77\)90025-9](https://doi.org/10.1016/0040-5809(77)90025-9).
24. Sharomi O, Malik T. Optimal control in epidemiology. *Ann Oper Res*. 2015;251(1–2):55–71. <https://doi.org/10.1007/s10479-015-1834-4>.
25. Behncke H. Optimal control of deterministic epidemics. *Optim Control Appl Methods*. 2000;21(6):269–85. <https://doi.org/10.1002/oca.678>.
26. Nowzari C, Preciado VM, Pappas GJ. Analysis and control of epidemics: a survey of spreading processes on complex networks. *IEEE Control Syst Mag*. 2016;36(1):26–46. <https://doi.org/10.1109/MCS.2015.2495000>.
27. Lenhart S, Workman JT. Optimal control applied to biological models. Boca Raton: Chapman & Hall/CRC Press; 2007. <https://doi.org/10.1201/9781420011418>.
28. Morton R, Wickwire KH. On the optimal control of a deterministic epidemic. *Adv Appl Probab* 1974;6(4):622–35. <https://doi.org/10.1017/s0001867800028482>.
29. Abakuks A. Optimal immunisation policies for epidemics. *Adv Appl Probab*. 1974;6(3):494–511. <https://doi.org/10.2307/1426230>.
30. Zaman G, Han Kang Y, Jung IH. Stability analysis and optimal vaccination of an SIR epidemic model. *Biosystems*. 2008;93(3):240–9. <https://doi.org/10.1016/j.biosystems.2008.05.004>.
31. Kar T, Batabyal A. Stability analysis and optimal control of an SIR epidemic model with vaccination. *Biosystems*. 2011;104(2):127–35. <https://doi.org/10.1016/j.biosystems.2011.02.001>.
32. Zaman G, Kang YH, Jung IH. Optimal treatment of an SIR epidemic model with time delay. *Biosystems*. 2009;98:43–50. <https://doi.org/10.1016/j.biosystems.2009.05.006>.
33. Liddo AD. Optimal control and treatment of infectious diseases. The case of huge treatment costs. *Mathematics*. 2016;4(2):21. <https://doi.org/10.3390/math4020021>.
34. Gaff H, Schaefer E. Optimal control applied to vaccination and treatment strategies for various epidemiological models. *Math Biosci Eng*. 2009;6:469–92. <https://doi.org/10.3934/mbe.2009.6.469>.
35. Hansen E, Day T. Optimal control of epidemics with limited resources. *J Math Biol*. 2011;62(3):423–51. <https://doi.org/10.1007/s00285-010-0341-0>.
36. Iacoviello D, Stasio N. Optimal control for sirc epidemic outbreak. *Comput Methods Programs Biomed*. 2013;110(3):333–42. <https://doi.org/10.1016/j.cmpb.2013.01.006>.
37. Bolzoni L, Bonacini E, Soresina C, Groppi M. Time-optimal control strategies in SIR epidemic models. *Math Biosci*. 2017;292:86–96. <https://doi.org/10.1016/j.mbs.2017.07.011>.
38. Barro M, Guiro A, Ouedraogo D. Optimal control of a SIR epidemic model with general incidence function and a time delays. *CUBO*. 2018;20(2):53–66. <https://doi.org/10.4067/s0719-06462018000200053>.
39. Bolzoni L, Bonacini E, Della Marca R, Groppi M. Optimal control of epidemic size and duration with limited resources. *Math Biosci*. 2019;315:108232. <https://doi.org/10.1016/j.mbs.2019.108232>.
40. Djidjou-Demasse R, Michalakis Y, Choisy M, Sofonea MT, Alizon S. Optimal COVID-19 epidemic control until vaccine deployment. *medRxiv* 2020. <https://doi.org/10.1101/2020.04.02.20049189>.
41. Perkins TA, España G. Optimal control of the COVID-19 pandemic with non-pharmaceutical interventions. *medRxiv* 2020. <https://doi.org/10.1101/2020.04.22.20076018>.
42. Kruse T, Strack P. Optimal control of an epidemic through social distancing. *SSRN Electron J* 2020;3581295. <https://doi.org/10.2139/ssrn.3581295>.
43. Ketcheson DI. Optimal control of an sir epidemic through finite-time non-pharmaceutical intervention. 2020. [arXiv:2004.08848](https://arxiv.org/abs/2004.08848).
44. Alvarez FE, Argente D, Lippi F. A simple planning problem for COVID-19 lockdown. Cambridge, MA. 2020. Tech. rep, NBER Working Paper No. 26981.
45. Bonnans JF, Gianatti J. Optimal control techniques based on infection age for the study of the COVID-19 epidemic. 2020. HAL-02558980v2.
46. Köhler J, Schwenkel L, Koch A, Berberich J, Pauli P, Allgöwer F. Robust and optimal predictive control of the COVID-19 outbreak. 2020. [arXiv:2005.03580](https://arxiv.org/abs/2005.03580).
47. Miclo L, Spiro D, Weibull J. Optimal epidemic suppression under an ICU constraint. 2020. [arXiv:2005.01327](https://arxiv.org/abs/2005.01327).
48. Charpentier A, Elie R, Laurière M, Tran VC. COVID-19 pandemic control: balancing detection policy and lockdown intervention under ICU sustainability. 2020. [arXiv:2005.06526](https://arxiv.org/abs/2005.06526).
49. Kermack WO, McKendrick AG, Walker GT. A contribution to the mathematical theory of epidemics. *Proc R Soc Lond A-CONTA*. 1927;115(772):700–21. <https://doi.org/10.1098/rspa.1927.0118>.
50. Hethcote HW. The mathematics of infectious diseases. *SIAM Rev*. 2000;42(4):599–653. <https://doi.org/10.1137/s0036144500371907>.
51. Brauer F. Compartmental models in epidemiology. In: *Mathematical epidemiology*. Berlin: Springer; 2008. p. 19–79. https://doi.org/10.1007/978-3-540-78911-6_2.
52. Epstein JM. Modelling to contain pandemics. *Nature*. 2009;460:687. <https://doi.org/10.1038/460687a>.
53. Rahmandad H, Sterman J. Heterogeneity and network structure in the dynamics of diffusion: comparing agent-based and differential equation models. *Manag Sci*. 2008;54(5):998–1014. <https://doi.org/10.1287/mnsc.1070.0787>.
54. Neher R, Aksamentov I, Noll N, Albert J, Dyrdak R. COVID-19 scenarios. Online (2020). https://github.com/neherlab/covid19_scenarios. Accessed on April 16, 2020

55. Noll NB, Aksamentov I, Druelle V, Badenhorst A, Ronzani B, Jefferies G, Albert J, Neher R. COVID-19 scenarios: an interactive tool to explore the spread and associated morbidity and mortality of SARS-CoV-2. medRxiv 2020. <https://doi.org/10.1101/2020.05.05.20091363>.
56. Wilson N, Telfar Barnard L, Kvalsig A, Verrall A, Baker MG, Schwehm M. Modelling the potential health impact of the COVID-19 pandemic on a hypothetical European country. medRxiv 2020. <https://doi.org/10.1101/2020.03.20.20039776>.
57. Neher RA, Dyrdak R, Druelle V, Hodcroft EB, Albert J. Potential impact of seasonal forcing on a SARS-CoV-2 pandemic. *Swiss Med Wkly.* 2020;150:w20224. <https://doi.org/10.4414/smw.2020.20224>.
58. Lloyd-Smith JO, Schreiber SJ, Kopp PE, Getz WM. Superspreading and the effect of individual variation on disease emergence. *Nature.* 2005;438:355–9. <https://doi.org/10.1038/nature04153>.
59. Diekmann O, Heesterbeek JAP, Metz JAJ. On the definition and the computation of the basic reproduction ratio R_0 in models for infectious diseases in heterogeneous populations. *J Math Biol.* 1990;28:365–82. <https://doi.org/10.1007/bf00178324>.
60. Shampine LF, Gladwell I, Shampine L, Thompson S. Solving ODEs with Matlab. Cambridge: Cambridge University Press; 2003. <https://doi.org/10.1017/cbo9780511615542>.
61. Richard Q, Alizon S, Choisy M, Sofonea MT, Djidjou-Demasse R. Age-structured non-pharmaceutical interventions for optimal control of COVID-19 epidemic. medRxiv 2020. <https://doi.org/10.1101/2020.06.23.20138099>.
62. Meyer-Hermann M, Pigeot I, Priesemann V, Schöbel A. Adaptive Strategien zur Eindämmung der COVID-19-Epidemie. 2020. Tech. rep, Accessed on July 13, 2020. https://www.mpg.de/14760567/28-04-2020_Stellungnahme_Teil_02.pdf.
63. Wiestler OD, Marquardt W, Heinz D, Meyer-Hermann M. Stellungnahme der Helmholtz-Initiative "Systemische Epidemiologische Analyse der COVID-19-Epidemie". (April 13, 2020) (2020). https://www.helmholtz.de/fileadmin/user_upload/01_forschung/Helmholtz-COVID-19-Papier_02.pdf. Accessed on April 17, 2020.
64. Robert Koch-Institute: Archiv der Situationsberichte des Robert Koch-Instituts zu COVID-19. Online (2020). https://www.rki.de/DE/Content/InfAZ/N/Neuartiges_Coronavirus/Situationsberichte/Archiv.html. Accessed on April 15, 2020
65. NPGeo Corona: RKI COVID19. Online (2020). https://npgeo-corona-npgeo-de.hub.arcgis.com/datasets/dd4580c810204019a7b8eb3e0b329dd6_0/. Accessed on April 16, 2020
66. Lauer SA, Grantz KH, Bi Q, Jones FK, Zheng Q, Meredith HR, Azman AS, Reich NG, Lessler J. The incubation period of coronavirus disease 2019 (COVID-19) from publicly reported confirmed cases: estimation and application. *Ann Intern Med.* 2020;172(9):577–82. <https://doi.org/10.7326/M20-0504>.
67. Koch-Institute R. (COVID-19). Online (2020). SARS-CoV-2 Steckbrief zur Coronavirus-Krankheit-2019. https://www.rki.de/DE/Content/InfAZ/N/Neuartiges_Coronavirus/Steckbrief.html. Accessed on April 14, 2020.
68. Verity R, Okell LC, Dorigatti I, Winskill P, Whittaker C, Imai N, Cuomo-Dannenburg G, Thompson H, Walker PGT, Fu H, Dighe A, Griffin JT, Baguelin M, Bhatia S, Boonyasiri A, Cori A, Cucunubá Z, FitzJohn R, Gaythorpe K, Green W, Hamlet A, Hinsley W, Laydon D, Nedjati-Gilani G, Riley S, van Elsland S, Volz E, Wang H, Wang Y, Xi X, Donnelly CA, Ghani AC, Ferguson NM. Estimates of the severity of coronavirus disease 2019: a model-based analysis. *Lancet Infect Dis.* 2020;20(6):669–77. [https://doi.org/10.1016/s1473-3099\(20\)30243-7](https://doi.org/10.1016/s1473-3099(20)30243-7).
69. Robert Koch-Institute: Täglicher Lagebericht des RKI zur Coronavirus-Krankheit-2019 (COVID-19): April 8, 2020. Online (2020). https://www.rki.de/DE/Content/InfAZ/N/Neuartiges_Coronavirus/Situationsberichte/2020-04-08-de.pdf. Accessed on April 14, 2020
70. German Interdisciplinary Society for Intensive Care Medicine (DIVI): DIVI Intensivregister. <https://www.divi.de/register/intensivregister>
71. Robert Koch-Institute: Täglicher Lagebericht des RKI zur Coronavirus-Krankheit-2019 (COVID-19): March 27, 2020. Online (2020). https://www.rki.de/DE/Content/InfAZ/N/Neuartiges_Coronavirus/Situationsberichte/2020-03-27-de.pdf. Accessed on April 14, 2020

Submit your manuscript to a SpringerOpen[®] journal and benefit from:

- Convenient online submission
- Rigorous peer review
- Open access: articles freely available online
- High visibility within the field
- Retaining the copyright to your article

Submit your next manuscript at ► [springeropen.com](https://www.springeropen.com)
